Biomimetic, Smart, and Multivalent Ligands for G-Quadruplex Isolation and Bioorthogonal Imaging

Francesco Rota Sperti, Thibaut Charbonnier, Pauline Lejault, Joanna Zell, Claire Bernhard, Ibai E Valverde, David Monchaud

Biomimetic, smart and multivalent ligands for G-quadruplex isolation and bioorthogonal imaging

Francesco Rota Sperti, Thibaut Charbonnier, Pauline Lejault, Joanna Zell, Claire Bernhard, Ibai E. Valverde* and David Monchaud*

ICMUB, CNRS UMR6302, UBFC Dijon, 9, Avenue Alain Savary, 21078 Dijon, France

E-mail : ibai.valverde@u-bourgogne.fr, david.monchaud@cnrs.fr

Abstract.

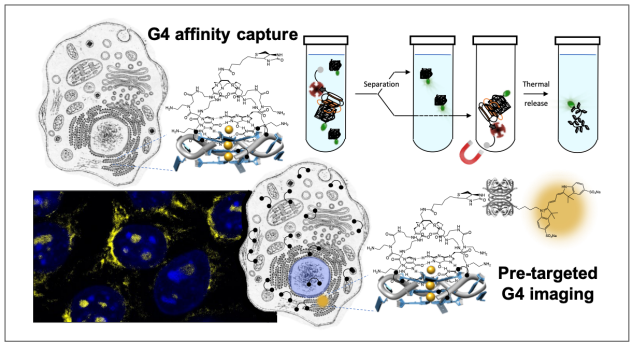

G-quadruplexes (G4s) continue to gather wide attention in the field of chemical biology as their prevalence in the human genome and transcriptome strongly suggests that they play key regulatory roles in cell biology. G4-specific, cell-permeable small molecules (G4-ligands) innovatively permit the interrogation of cellular circuitries in order to assess to what extent G4s influence cell fate and functions. Here, we report on multivalent, biomimetic G4-ligands referred to as TASQs that enable both the isolation and visualization of G4s in human cells. Two biotinylated TASQs, **BioTASQ** and **BioCyTASQ**, are indeed efficient molecular tools to isolate G4s from mixtures of nucleic acids through simple affinity capture protocols and to image G4s in cells *via* a biotin/avidin pre-targeted imaging system first applied here to G4s, found to be a reliable alternative to *in situ* click chemistry.

Introduction

The principle of template-assembled synthetic proteins (TASP)[1, 2] was developed by Mutter to tackle the issue of controlling polypeptide folding into functional protein-like macromolecules. Inspired by this principle, Sherman reported on template-assembled synthetic G-quartets (TASQ)[3] to show how discrete G-quartets can be assembled intramolecularly. To this end, four guanine residues were covalently linked to a template, resulting in a conformationally

dynamic suprastructure in which the guanines can be either independent of each other (the so-called 'open' conformation of TASQ, figure 1) or assembled into a G-quartet (*via* the formation of 8 hydrogen bonds, the 'closed' conformation).

The first prototypes of TASQ were built on a lipophilic template (Cram's bowl-shape cavitands[4] with long alkyl chains) in order to study the cation (Na^+, K^+, Sr^{2+}) chelation properties of discrete, synthetic G-quartets in organic media ($CHCl_3$).[3, 5, 6] Soon after, water-soluble TASQs were developed, hinging on hydrophilic templates such as the polyazamacrocyclic DOTA for the **DOTASQ**,[7, 8] the cyclodecapeptide RAFT (regioselectively addressable functionalized template, initially introduced by Mutter for the synthesis of TASP)[2, 9, 10] for the **RAFT-G4**,[11] as well as cavitands with phosphate appendages.[12, 13] This opened new possibilities for the design of biomimetic G-quadruplex ligands (or G4-ligands,[14, 15] *vide infra*) applicable in cells, or of molecular platforms to evaluate the G-quartet interacting properties of G4-ligands *in vitro*.[13, 16, 17]

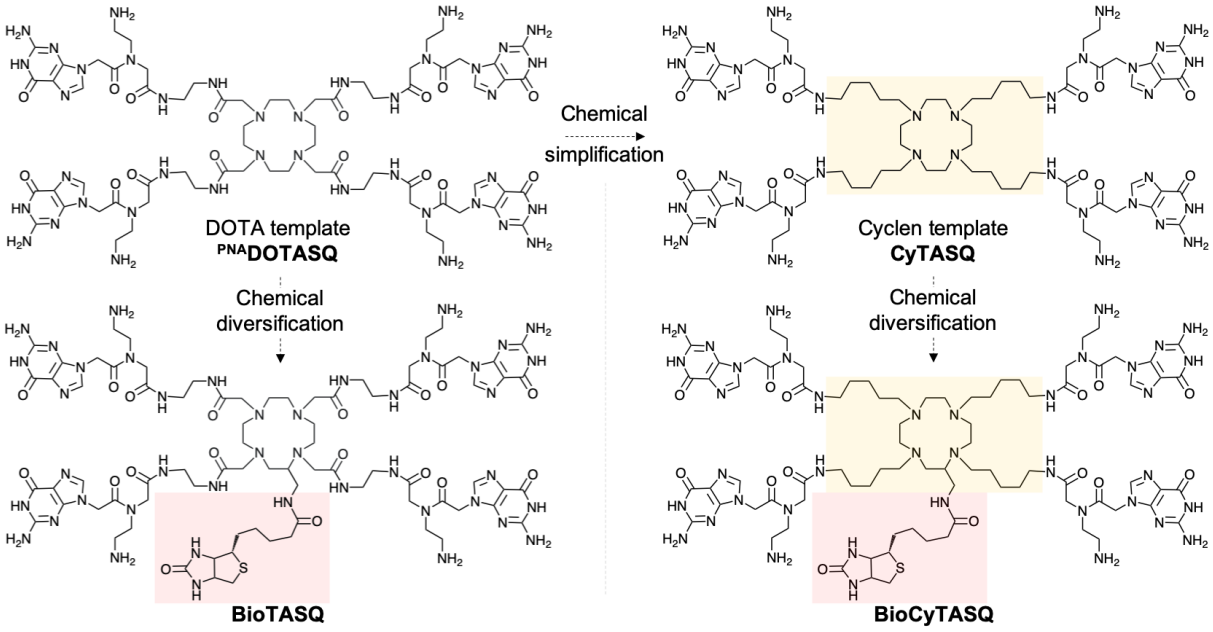

Figure 1. Structures of the DOTA-based ^{PNA}DOTASQ and BioTASQ and the cyclen-based CyTASQ and BioCyTASQ.

We have been particularly interested in fine-tuning the chemical scaffold of water-soluble TASQ in order to optimize their properties as biomimetic G4-ligands. The main binding site of a small-molecule within the G4 architecture is the external, accessible G-quartet.[18] Since a G4 is more stable with more constitutive G-quartets,[19] we set out to synthesize TASQ to interact with G4s according to such a biomimetic, like-likes-like interaction between a native G4

quartet and the synthetic TASQ quartet. By doing so, we have gradually modified the chemical nature of TASQ from the first biomimetic G4-ligand (**DOTASQ**,[7, 20] and **PorphySQ**)[21] to the first smart G4-ligands ^{PNA}**DOTASQ**[22, 23] (Figure 1) and ^{PNA}**PorphySQ**,[24] whose closed conformation is triggered only by interaction with G4s, twice-as-smart G4-ligands **PyroTASQ**[25, 26] and **N-TASQ**,[27, 28] smart ligands and smart probes, used to detect G4s *in vitro* and *in cella*, and the multivalent G4-ligand **BioTASQ**[29, 30] (Figure 1), used as molecular bait for isolating G4 from human cells and identifying them by sequencing.

A critical bottleneck in the development of TASQ resides in their chemical accessibility. Despite their relatively short synthesis, some technical pitfalls preclude efficient large-scale synthesis. We thus decided to revisit the synthesis of TASQ and report herein on the synthesis of both cyclen-template synthetic G-quartet (**CyTASQ**) and its biotinylated counterpart **BioCyTASQ** (Figure 1), whose design was inspired by that of the reference compound ^{PNA}**DOTASQ** and **BioTASQ**,[22, 29, 30] but with a simpler chemical scaffold and less time-consuming chemical accessibility.

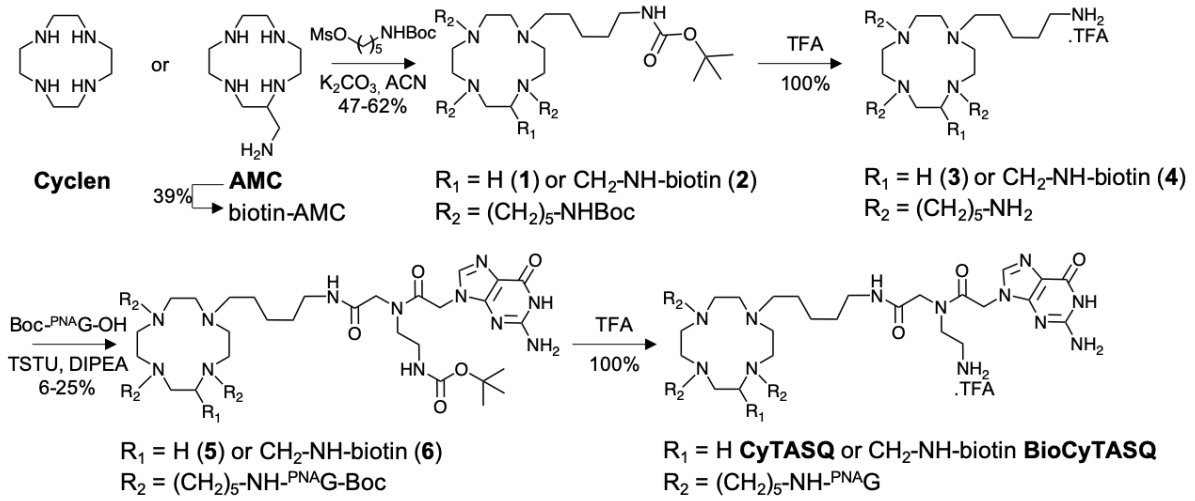

Figure 2. Chemical synthesis of CyTASQ and BioCyTASQ.

Design & synthesis of CyTASQ and BioCyTASQ. These two new TASQs were designed with the same global structural organization as ^{PNA}**DOTASQ** and **BioTASQ** (Figure 1), changing the topologically constrained amide linkers for more flexible alkyl linkers of similar length (in terms of number of atoms). This replacement, although conceptually simple, results in a more straightforward accessibility to the final TASQ with increased overall chemical yields (from 0.6% to 6% for **BioTASQ** and **BioCyTASQ**, respectively, Figure 2). Briefly, the starting material

for the synthesis of **CyTASQ** (Figures 2 and S1-S5) is the commercially available cyclen while that of **BioCyTASQ** (Figures 2 and S6-S11) is a biotinylated aminomethylcyclen (biotin-AMC),[29, 30] prepared in one step (39% chemical yield) from AMC.[31] These polyazamacrocycles were reacted with an excess (8 mol. equiv.) of 5-(Boc-amino)pentyl mesylate (prepared in two steps from the commercially available 5-amino-1-pentanol, 56% yield) in presence of potassium carbonate (K_2CO_3) in acetonitrile (ACN) to give compounds **1** (47% yield) and **2** (62% yield). These intermediates were deprotected with trifluoroactetic acid (TFA) to afford compounds **3** and **4** (100% yield), which were subsequently coupled with an excess (4.4 mol. equiv.) of Boc-^{PNA}G-OH monomers (prepared in one step from the commercially available Boc-^{PNA}G(Z)-OH, 72%) in presence of *N*,*N*,*N'*,*N'*-tetramethyl-O-(*N*-succinimidyl)uronium tetrafluoroborate (TSTU) and diisopropylethylamine (DIPEA) to afford the protected TASQs **5** (6% yield) and **6** (25% yield). The final compounds, **CyTASQ** and **BioCyTASQ**, were obtained in a final, quantitative deprotection step (TFA).

Evaluation of G4-interacting properties of CyTASQ and BioCyTASQ *in vitro*. The apparent affinity of TASQs for different DNA/RNA sequences was evaluated *via* the firmly established FRET-melting assay (Figure 3A).[32, 33] Doubly labelled biologically relevant G4-forming DNA/RNA sequences[34] (0.2 μM) were heated from 20 to 90 °C in the presence of TASQs (1.0 μM). The sequences used were the human telomeric-mimicking F-21-T (FAM-d[$^{5'}G_3(T_2AG_3)_3{}^{3'}$]-TAMRA; FAM for fluorescein amidite, TAMRA for tetramethylrhodamine), the Myc promoter-mimicking F-Myc-T (FAM-d[$^{5'}GAG_3TG_4AG_3TG_4A_2G^{3'}$]-TAMRA), the human telomeric transcript F-TERRA-T (FAM-r[$^{5'}G_3(U_2AG_3)_3{}^{3'}$]-TAMRA) and the 5'-UTR of the mRNA coding for VEGF (F-VEGF-T, FAM-r[$^{5'}G_2AG_2AG_4AG_2AG_2A^{3'}$]-TAMRA), along with F-duplex-T as a control (the hairpin-forming FAM- d[$^{5'}(TA)_2GC(TA)_2T_6(TA)_2GC(TA)_2{}^{3'}$]-TAMRA). As seen in figure 3A, the mid-transition temperatures ($T_{1/2}$, expressed in °C) of all DNA/RNA G4s increased in the presence of TASQs, although to a varying extent with $\Delta T_{1/2}$ (= [$T_{1/2}$(G4+ligand) - $T_{1/2}$(G4)]) ranging from 1.0 and 21.8 °C. The chemical simplification of the G arms (**CyTASQ** *versus* **^{PNA}DOTASQ** and **BioCyTASQ** *versus* **BioTASQ**) affects the TASQ G4-stabilizing properties differently: on one hand, the stabilizations induced by **^{PNA}DOTASQ** (black bars, $\Delta T_{1/2}$ between 12.0 and 21.2 °C) are systematically higher than that of **CyTASQ** (brown bars, $\Delta T_{1/2}$ = 5.2 - 10.0 °C); on the other hand, the **BioTASQ** stabilization values (gray bars, $\Delta T_{1/2}$ = 1.0 - 2.7 °C) are

systematically lower than that of **BioCyTASQ** (red bars, $\Delta T_{1/2}$ = 4.7 - 10.0 °C), comparable to that of **CyTASQ**.

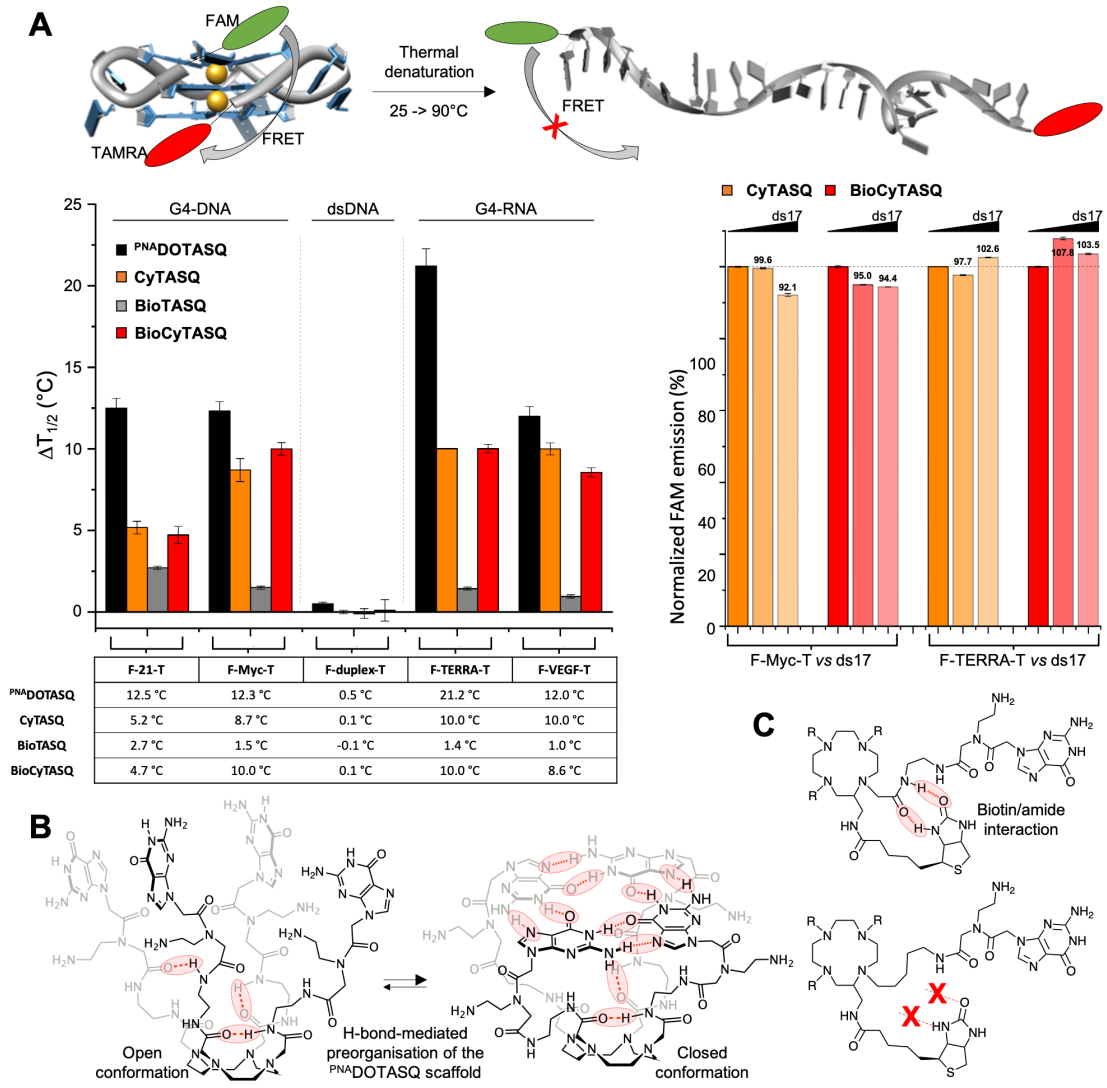

	F-21-T	F-Myc-T	F-duplex-T	F-TERRA-T	F-VEGF-T
PNADOTASQ	12.5 °C	12.3 °C	0.5 °C	21.2 °C	12.0 °C
CyTASQ	5.2 °C	8.7 °C	0.1 °C	10.0 °C	10.0 °C
BioTASQ	2.7 °C	1.5 °C	-0.1 °C	1.4 °C	1.0 °C
BioCyTASQ	4.7 °C	10.0 °C	0.1 °C	10.0 °C	8.6 °C

Figure 3. **A**. Schematic representation of the FRET-melting assay (upper panel) and results ($\Delta T_{1/2}$, in °C) collected with doubly labelled G4s (DNA: F-21-T, F-Myc-T; RNA: F-VEGF-T, F-TERRA-T) and a duplex as a control (F-duplex-T) in the presence of TASQ (^{PNA}DOTASQ in black, CyTASQ in brown, BioTASQ in gray and BioCyTASQ in red) (lower panel, left), results of competitive FRET-melting experiments (lower panel, right) performed with doubly labelled G4-DNA (F-Myc-T) or G4-RNA (F-TERRA-T) in presence of TASQ (CyTASQ in brown, BioCyTASQ in red) and increasing amounts of unlabelled duplex-DNA competitor (ds17, 15 and 50 molar equiv.). **B**,**C**. Schematic representation of possible intramolecular H-bonds in the ^{PNA}DOTASQ scaffold (left panel), and between the biotin appendage and either the BioTASQ or the BioCyTASQ arm (right panel).

These results could be interpreted mostly in terms of flexibility of the G arms: the alkyl arms of **CyTASQ** and **BioCyTASQ** have a far greater flexibility than the amide arms of **^{PNA}DOTASQ** and **BioTASQ**. Surprisingly, this flexibility, which should provide TASQs with a greater conformational adaptability to their G4 targets, decreases the performances of the non-

biotinylated TASQs, **CyTASQ** being less efficient than **^{PNA}DOTASQ**. This implies that the amide connection in the arms of **^{PNA}DOTASQ** somehow pre-organizes it, presumably *via* the creation of internal H-bonds (Figure 3B), as already investigated *in silico* (MM3 force field) with the parent compound **DOTASQ**.[7] On the other hand, this flexibility improves the performances of biotinylated TASQs, **BioCyTASQ** being more efficient than **BioTASQ**: we initially postulated that biotin poisons **BioTASQ**'s G4 affinity by H-bonding one of its Gs (**BioTASQ v.1** *versus* **v.2**);[30] our new results suggest that biotin might primarily interact with the amide connector of the G arm (Figure 3C), an internal interaction that is not possible in the **CyTASQ**/**BioCyTASQ** series, explaining why these two TASQs display similar performances. These new results thus confirm that the flexible alkyl arms of **CyTASQ** and **BioCyTASQ** make them less structurally preorganized than **^{PNA}DOTASQ** (lower apparent affinity) but also less internally poisoned than **BioTASQ** (higher apparent affinity).

This series of FRET-melting experiments also shows that TASQs do not interact with duplex-DNA (with $\Delta T_{1/2}$ < 0.5 °C). This G4-specificity was further confirmed by competitive FRET-melting assays performed with F-Myc-T and F-TERRA-T (0.2 μM) in the presence of **BioTASQ**/**BioCyTASQ** (1.0 μM) and an excess of the unlabelled duplex-DNA competitor ds17 (d[$^{5'}C_2AGT_2CGTAGTA_2C_3{}^{3'}$]/d[$^{5'}G_3T_2ACTACGA_2CTG_2{}^{3'}$]). The new TASQs are highly G4-specific (Figure 3C) with a maintained stabilization of >92% for **CyTASQ** and >98% for **BioCyTASQ**. The high affinity and exquisite selectivity of the biotinylated **BioCyTASQ** makes it well suited to be used as a molecular bait for isolating G4s from nucleic acids mixtures.

Evaluation of G4-capture properties of CyTASQ and BioCyTASQ *in vitro*. The ability of the biotinylated TASQs to pull down G4s was assessed *via* an optimized version of the 'pull-down' or 'affinity capture' protocol[35] adapted for the **BioTASQ** (Figure 4A).[30] FAM-labelled G4-forming DNA/RNA sequences (1 μM) were incubated for 2 h at room temperature with either **BioTASQ** or **BioCyTASQ** (10 μM) in presence of streptavidin-coated magnetic beads in TrisHCl buffer (20mM, pH 7.2) containing 1 mM KCl, 99 mM LiCl and 10 mM $MgCl_2$ (this KCl/LiCl ratio, which corresponds to the FRET-melting buffers, ensures proper G4 stability at 25 °C; the Mg^{2+} decreases the non-specific electrostatic interactions between DNA and TASQs). The G4-forming sequences used were the human telomeric-mimicking F-22AG (FAM-d[$^{5'}AG_3(T_2AG_3)_3{}^{3'}$]), a section of the promoters of MYC (FAM-d[$^{5'}GAG_3TG_4AG_3TG_4A_2G^{3'}$]) and SRC genes (FAM-d[$^{5'}G_3AG_3AG_3CTG_5{}^{3'}$]), and F-duplex as a control (FAM-

d[$^{5'}$(TA)$_2$GC(TA)$_2$T$_6$(TA)$_2$GC(TA)$_2$$^{3'}$]). The FAM-G4/**TASQ**/beads assemblies were isolated (magnetic immobilization), the supernatant removed and the FAM-G4 resuspended in solution after a thermal denaturation step (10 min at 90 °C). The capture/release efficiency of TASQ was quantified by the FAM emission of the resulting solution, normalized to the controls performed without TASQ.

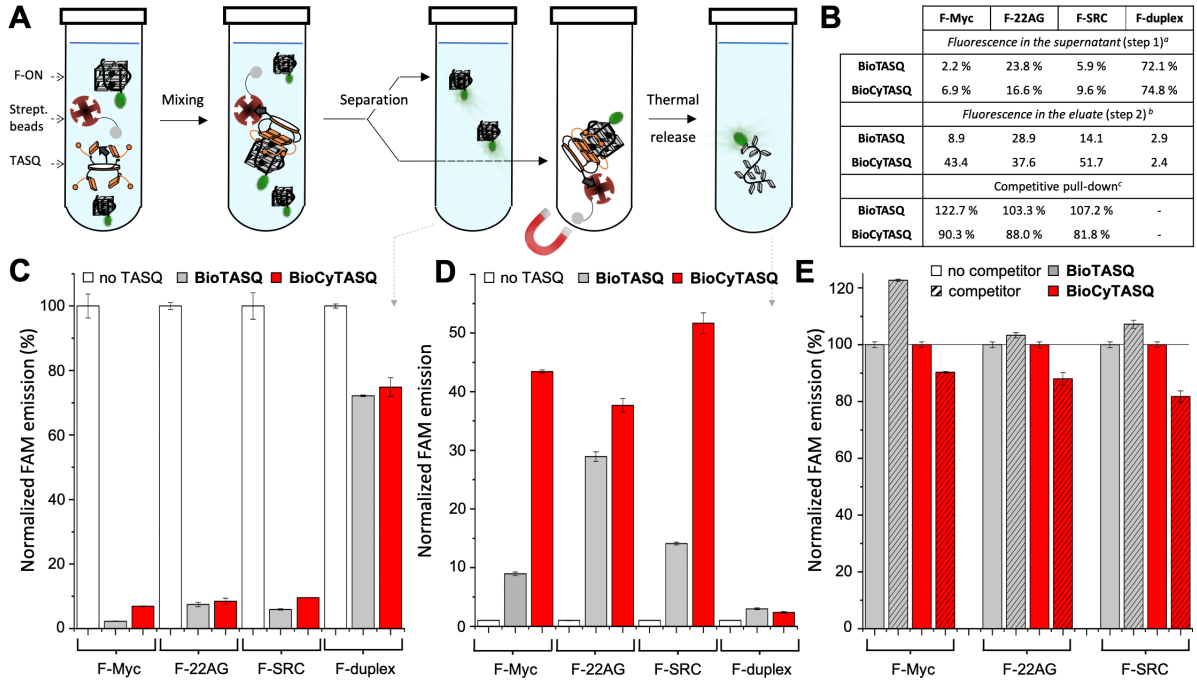

	F-Myc	F-22AG	F-SRC	F-duplex
	Fluorescence in the supernatant (step 1)[a]			
BioTASQ	2.2 %	23.8 %	5.9 %	72.1 %
BioCyTASQ	6.9 %	16.6 %	9.6 %	74.8 %
	Fluorescence in the eluate (step 2)[b]			
BioTASQ	8.9	28.9	14.1	2.9
BioCyTASQ	43.4	37.6	51.7	2.4
	Competitive pull-down[c]			
BioTASQ	122.7 %	103.3 %	107.2 %	-
BioCyTASQ	90.3 %	88.0 %	81.8 %	-

Figure 4. **A**. Schematic representation (**A**) and results (**B**) of the *in vitro* G4 pull-down protocol performed with FAM-labelled oligonucleotides (the G4s F-Myc, F-22AG and F-SRC; the hairpin F-duplex) and either **BioTASQ** or **BioCyTASQ** quantified by either the decrease in fluorescence of the supernatant (step 1, **C**; [a]with respect to the control F-ON+beads without TASQ normalized at 100 %) or the increase in fluorescence during the elution (step 2, **D**; [b]in fold-change, normalized to the control (without TASQ) normalized to 1). Competitive pull-down experiments (**E**) performed with F-Myc, F-22AG and F-SRC, **BioTASQ** or **BioCyTASQ** and the unlabelled duplex competitor ds12 ([c]with 20 mol. equiv. ds12, with respect to the control (without ds12) normalized at 100 %).

Both **BioTASQ** and **BioCyTASQ** efficiently captured G4s in solution (Figures 4B-E). This could be assessed by both the decrease in FAM intensity of the supernatant, which reflects the pull-down *per se* (with a pull-down efficiency as low as -98 % as compared to the control, *i.e.*, experiments performed without TASQ, normalized to 100%, panel C) and the increase in FAM intensity after releasing the beads content by a thermal denaturation step (with a release enrichment up to 52-fold as compared to the control, *i.e.*, experiments performed without TASQ, normalized to 1, panel D). The results obtained again demonstrate the improved performances of **BioCyTASQ** (red bars) in comparison with **BioTASQ** (gray bars) during the elution step (9- *versus* 44-, 29- *versus* 38- and 14- *versus* 52-fold enrichment for F-Myc, F-22AG

and F-SRC, respectively). This difference in efficiency likely originate in a better overall G4 affinity of **BioCyTASQ**, and insights obtained by CD titrations (Figure S12) tend to confirm than it binds more avidly to folded G4s (in line with the results depicted in Figure 3A and obtained with the highly stable F-Myc and F-SRC, Figure 4D), while **BioTASQ** interacts more strongly with partly folded G4s to help them fold (in line with the results obtained with the F-22AG, Figure 4D, which is less stably folded than F-Myc and F-SRC in the conditions of the pull-down assay). Again, these results also show that TASQs are specific for G4s (see the control with F-duplex, with 2- and 3-fold enrichment), a specificity further confirmed by competitive pull-down experiments performed with F-Myc, F-22AG and F-SRC (1 μM) in the presence of either **BioTASQ** or **BioCyTASQ** (10 μM) and an excess (20 μM) of an unlabelled duplex-DNA competitor ds12 (the self-complementary strands d[$^{5'}$CGCGA$_2$T$_2$CGCG$^{3'}$]), in which the pull-down efficiency is maintained at >82% for **BioTASQ** and >103% for **BioCyTASQ** (Figure 4E).

Evaluation of G4-interacting properties of CyTASQ and BioCyTASQ *in cella*. The biotin appendage of both **BioTASQ** and **BioCyTASQ** can also be used for optical imaging. Inspired by pre-targeted imaging and therapy strategies involving biotin- and/or streptavidin-antibody conjugates,[36-38] we used both **BioTASQ** and **BioCyTASQ** for imaging G4s in human cancer cells (MCF7) based on the highly specific interaction between the biotin appendage of TASQ and a Cy3-labelled streptavidin (SA-Cy3). Two strategies were implemented, with a systematic comparison of the properties of **BioTASQ** and **BioCyTASQ**: a post-fixation or a live-cell labelling strategy. In the first strategy, MCF7 cells are fixed (cold MeOH) then incubated sequentially with either **BioTASQ** or **BioCyTASQ** (1 μM, 1 h), SA-Cy3 (1 μg/mL) and DAPI (2.5 μg/mL) (Figure 5A). In the second strategy, MCF7 cells are treated live with either **BioTASQ** or **BioCyTASQ** (1 μM, 24 h; IC_{50} >100 μM) before fixation (cold MeOH), and sequential SA-Cy3 and DAPI labelling (Figure 5B). Both strategies are intended to provide complementary outputs as the former leads to a snapshot of G4 landscapes as captured by chemical fixation while the latter highlights cellular sites where TASQs accumulate in live cells.

In both instances, **BioCyTASQ** provided a brighter response than **BioTASQ** (Figure 5, the images were collected and treated under strictly identical setups). Post-fixation labelling led to a rather diffuse labelling in the cytoplasm along with stronger labelling in perinuclear regions (yellow arrows), nucleoli (white arrows) and non-nucleoli nucleoplasmic sites (red arrows). Live-cell labelling provided a similar perinuclear/nucleoli/nuclear distribution but

with a higher contrast, with abundant G4-RNA sites, mostly found in ribosome sites (nucleoli (white arrows) and rough endoplasmic reticulum (yellow arrows)) and sparser G4-DNA sites (located in the nucleoplasm (red arrows)). These results, in full agreement with the direct G4 labelling pattern observed with N-TASQ,[27, 28, 39, 40] complies with the known G4-richness of ribosomal sites.[41-44] We observe that the live-cell treatment shows a similar staining pattern to post-fixation labelling, indicating the G4 landscape is not drastically redistributed by TASQ treatment (mostly due to their low ability to artificially promote G4-formation (*vide supra*), in line with their smart ligand nature). Live cell imaging, which is more accurate because the ligand's target is not chemically altered by fixation, should thus be preferred to investigate G4 biology with TASQs. To the best of our knowledge, this is the first description of a pre-targeted imaging strategy based on the biotin/avidin system applied to visualize G4s in human cells.

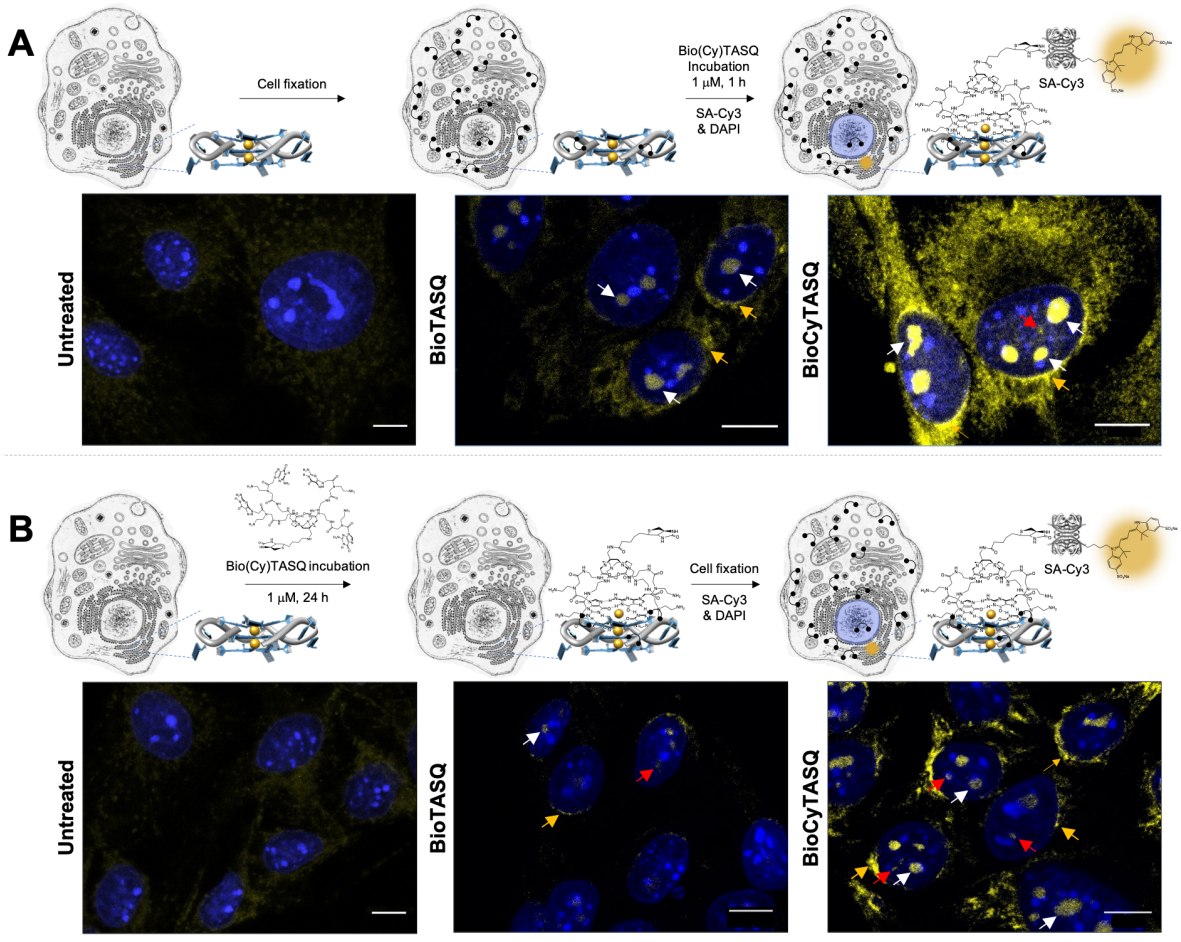

Figure 5. Schematic representation (and microscopy images) of the **BioTASQ**/**BioCyTASQ**-based, two-step strategies implemented to label G4s in MCF7 cells, either (**A**) post-fixation or (**B**) live-cell labelling. Images are collected in the range of 518-562 nm for SA-Cy3 (yellow) and < 425 nm for DAPI (blue channel); scale bar 10 μm; yellow, white and red arrows indicate G4 *foci* found in perinuclear regions, nucleoli and nucleoplasm, respectively.

Conclusion

The panel of strategies now applicable to gaining insights into G4 landscapes within human cells encompasses optical imaging[45, 46] and sequencing methods.[47, 48] These strategies rely on exquisitely efficient and specific molecular tools to either label G4 sites within cells (*e.g.*, direct labelling with G4 probes or indirect labelling *via* bioorthogonal chemistry)[45, 46, 49, 50] or stabilize G4s *in vitro*, thus causing polymerase stalling which is used as a next-generation sequencing readout (*e.g.*, pyridostatin in G4-seq[51] and rG4-seq[52] protocols).[47, 48, 53] In light of the number of potential G4-forming sequences in the human genome and transcriptome,[51, 54-60] and the variety of biological processes they might be involved in,[34, 61-64] the task can seem daunting; however, this offers a virtually unlimited playground for chemical biology investigation, as every new tool and approach could provide alternative and/or complementary information helping to further decipher the complex biology of G4s.

Here, we continue to exploit the potential of biomimetic and smart G4 ligands, demonstrating the versatility of biotinylated TASQs to both isolate G4s by pull-down affinity capture, implementable in cells by G4RP-seq for instance, [27] and visualize G4s *via* an original streptavidin/biotin pretargeted imaging approach, found to be a reliable alternative to *in situ* click chemistry.[50] We address the problem of poor chemical accessibility of TASQs *via* the design and synthesis of the new generation TASQs referred to as **CyTASQ** and **BioCyTASQ**, which can now be produced on scales and timescales compatible with a broader use. The *in vitro* validation provided here lends further credence to the relevance of TASQs as multivalent molecular tools to investigate G4s *in cella,* endowing them with new functionalities that continue to demonstrate their versatility.

Methods

A fully detailed Material and Methods part is provided in the Supporting Information, including the synthesis and characterization of **CyTASQ** (Figures S1-S5), additional characterizations for **BioCyTASQ** (Figures S6-S11) and the preparation of the oligonucleotides used in this study. Details regarding the synthesis and characterization of **BioCyTASQ** (depicted in Figure 2) and the protocols of FRET-melting assays (results seen in Figure 3), pull-down assay (Figure 4) and pretargeted imaging (Figure 5) are provided below:

Synthesis of BioCyTASQ.

Biotin-AMC: To a solution of biotin (514.7 mg, 2.10 mmol, 0.8 equiv.) and DIPEA (949 µL, 5.40 mmol, 2.0 equiv.) in DMF (10 mL) was added TSTU (900 mg, 3.00 mmol, 1.1 equiv.) and the solution was stirred at RT until the complete activation of the carboxylic acid, assessed *via* HPLC-MS monitoring. The solution was then added dropwise (1 mL/3 h) to a solution of AMC (546 mg, 2.70 mmol, 1.0 equiv.) in DMF (20 mL) and the reaction was carefully monitored by HPLC-MS. Upon completion, TFA (500 µL) was added and the solution was concentrated under vacuum and the resulting residue purified by RP-HPLC in a H_2O/can + 0.1% TFA mixture (gradient of 2 to 100 % over 50 min). Compound **Biotin-AMC** was obtained after removal of the solvents by lyophilization (926 mg, 1.04 mmol, 39% yield). ^{1}H NMR (500 MHz, D_2O) δ 4.60 (dd, *J* = 8.0, 4.9 Hz, 1H), 4.41 (dd, *J* = 8.0, 4.5 Hz, 1H), 3.45-3.36 (m, 2H), 3.35-3.31 (m, 1H), 3.21-2.92 (m, 16H), 2.79-2.76 (m, 1H), 2.30 (t, *J* = 7.5 Hz, 2H), 1.76-1.52 (m, 4H), 1.46-1.36 (m, 2H), 1.34-1.32 (m, 2H) (signals of intracyclic amines and amide are missing due to proton solvent exchange). ^{13}C NMR: (126 MHz, D_2O) δ 177.7, 165.3, 62.1, 60.3, 55.4, 52.0, 46.3, 44.4, 44.2, 44.0, 42.6, 42.1, 40.3, 39.7, 39.13, 39.09, 35.3, 28.0, 27.7, 24.9, 17.7, 16.2. ESI-MS: $[M+H]^+$ m/z = 428.4 (calcd. for $C_{19}H_{38}N_7O_2S$: 428.6). HPLC-MS characterization (Phenomenex Kinetex C18 column, 2.6µm, 2.1 × 50 mm) *via Method A* (from 5% to 100% MeCN/H_2O+0.1% formic acid (FA) in 7 min): retention time = 0.373 min; purity: >90% at 201 nm, >98% at 214 nm; m/z = 428.4 $[M+H]^+$ (cf. Figure S7).

Compound **2**: To a solution of compound **Biotin-AMC** (283.2 mg, 0.32 mmol, 1.0 equiv.) in acetonitrile (4 mL) was added 5-((tert-butoxycarbonyl)amino)pentyl methanesulfonate (720 mg, 2.56 mmol, 8.0 equiv.) and K_2CO_3 (472 mg, 3.42 mmol, 10.0 equiv.) and the solution was stirred at 50°C for 56 h. Another aliquot of 5-((tert-butoxycarbonyl)amino)pentyl methanesulfonate (392 mg, 1.40 mmol, 4.0 equiv.) was added and further stirred for 16 h. The crude mixture was filtered and concentrated under vacuum and the residue was purified by HPLC in a H_2O/ACN + 0.1% TFA mixture (gradient of 30 to 100 % over 40 min). Compound **2** was obtained after removal of the solvents by lyophilization (232.5 mg, 0,20 mmol, 62% yield). ^{1}H NMR: (500 MHz, DMSO-d_6) δ 8.01 (br s, 1H), 7.86-7.69 (m, 2H), 6.81-6.79 (m, 3H), 6.40 (br s, 1H), 4.32 (dd, *J* = 5.0, 7.0 Hz, 1H), 4.20-4.16 (m, 2H), 4.13 (dd, *J* = 4.5, 7.5 Hz, 1H), 3.48-3.36 (m, 4H), 3.17-2.57 (m, 36H), 2.11-2.08 (m, 2H), 1.69-1.21 (m, 60H). ^{13}C NMR: (126 MHz, DMSO-d_6) δ 206.5, 162.7, 155.65, 155.61, 77.4, 70.4, 70.2, 61.1, 59.2, 55.4,52.5, 51.8, 39.6 (3 C), 38.61, 36.4, 35.1, 30.7, 29.0, 28.0, 26.9, 25.8, 25.2, 24.0, 23.4, 22.2, 21.1. MALDI: $[M+H]^+$

1169.0 m/z = (calcd. for $C_{59}H_{114}N_{11}O_{10}S$: 1168.8). HPLC-MS characterization (*Method A*): retention time = 4.06 min; purity: >99% at 201 nm, >95% at 214 nm; m/z = 385.1 $[M+H]^{3+}$ and 1169.0 $[M+H]^{+}$ (cf. Figure S8).

Compound **4**: compound **2** was stirred in 1 mL of TFA for 1 hour. After evaporation of the TFA, compound **4** was obtained (78.5 mg, 0.08 mmol, 100 % yield), ESI-MS: $[M+H]^{+}$ m/z = 768.6. (calcd. for $C_{39}H_{81}N_{11}O_2S$: 768.6). HPLC-MS characterization (*Method A*): retention time = 0.34 min; purity: >94% at 201 nm, >94% at 214 nm; m/z = 385.0 $[M+H]^{2+}$ and 768.6 $[M+H]^{+}$ (cf. Figure S9).

Compound **6**: Boc-^{PNA}G-OH (245 mg, 0.63 mmol, 4.8 equiv.), TSTU (191 mg, 0.63 mmol, 4.8 equiv.) were dissolved in DMF (1.5 mL) and DIPEA was added (99 µL, 0.63 mmol, 4.8 equiv.). After the complete activation of the carboxylic acid (HPLC-MS monitoring), a solution of compound **5** (100 mg, 0.13 mmol, 1.0 equiv.) and DIPEA (44 µL, 0.26 mmol, 2.0 equiv.) in DMF (1.5 mL) was added. The mixture was stirred at RT overnight. The solution was then concentrated under vacuum and the residue was purified by RP-HPLC in a H_2O/ACN + 0.1% TFA mixture (gradient of 15 to 65 % over 50 min). Compound **6** was obtained after removal of the solvents by lyophilization (77.8 mg, 0.03 mmol, 25% yield). ^{1}H NMR: (500 MHz, DMSO-d_6) δ 10.76-10.71 (m, 4H), 8.31-8.27 (m, 3H), 8.03-7.85 (m, 5H), 7.67-7.64 (m, 4H), 7.20-6.99 (m, 4H), 6.78-6.65 (m, 4H), 6.50-6.41 (m, 8H), 4.96-4.82 (m, 8H), 4.33-4.30 (m, 2H), 4.13-4.11 (m, 6H), 4.00-2.59 (m, 53H), 2.10 (br s, 2H), 1.60-1.14 (m, 62H). ESI-HRMS: $[M+H+Na]^{2+}$ m/z = 1178.63633 (calc. for $[C_{103}H_{166}N_{39}O_{22}SNa]^{2+}$: = 1178.63519). HPLC-MS characterization (*Method A*): retention time = 3.62 min; purity: >98% at 201 nm, >97% at 214 nm, >99% at 280 nm; m/z = 1168.0 $[M+2H]^{2+}$ (cf. Figure S8); *via Method B* (from 5% to 15% MeCN/H_2O+0.1% FA in 5 min, from 15% to 70% MeCN/ H_2O+0.1% FA in 20 min, from 70% to 100% MeCN/ H_2O+0.1% FA in 3 min): retention time = 11.68 min; purity: >93% at 280 nm (cf. Figure S10).

BioCyTASQ: compound **6** was dissolved in 1 mL of TFA and stirred for 1 hour. The complete deprotection was assessed by HPLC-MS (*Method A*): retention time = 0.33 min; m/z = 968.0 $[M+2H]^{2+}$. TFA was removed under reduced pressure, the residue lyophilized and used without further purification. ESI-HRMS: $[M+2H]^{2+}$ m/z = 967.04040 (calc. for $[C_{83}H_{136}N_{39}O_{14}S]^{2+}$: =967.03802). HPLC-MS (*Method A*): retention time = 0.33 min; purity: >91% at 214 nm, >94% at 254 nm, >97% at 280 nm; m/z = 968.0 $[M+2H]^{2+}$ (cf. Figure S11).

FRET-melting assays.

FRET-melting experiments were performed in a 96-well format using a Mx3005P qPCR machine (Agilent) equipped with FAM filters (λ_{ex} = 492 nm; λ_{em} = 516 nm) in 100 μL (final volume) of 10 mM lithium cacodylate buffer (pH 7.2) plus 10 mM KCl/90 mM LiCl (F21T, F-duplex-T) or plus 1 mM KCl/99 mM LiCl (F-Myc-T, F-Terra-T, F-VEGF-T) with 0.2 μM of labeled oligonucleotide and 1 μM of TASQ. Competitive experiments were carried out with labeled oligonucleotide (0.2 μM), 1 μM TASQ and increasing amounts (0, 15 and 50 equiv.) of the unlabeled competitor ds17. After an initial equilibration step (25°C, 30 s), a stepwise increase of 1°C every 30s for 65 cycles to reach 90°C was performed, and measurements were made after each cycle. Final data were analyzed with Excel (Microsoft Corp.) and OriginPro®9.1 (OriginLab Corp.). The emission of FAM was normalized (0 to 1), and $T_{1/2}$ was defined as the temperature for which the normalized emission is 0.5; $\Delta T_{1/2}$ values are means of 3 experiments.

Pull-down assay.

The streptavidin MagneSphere® beads (Promega) were washed 3 times with TrisHCl buffer containing 1 mM KCl, 99 mM LiCl and 10 mM $MgCl_2$. Either **BioTASQ** or **BioCyTASQ** (10 μM) was mixed with 5'-labeled oligonucleotides (F-ON, 1 μM), *i.e.*, F-Myc, F-SRC, F-22AG and F-duplex, MagneSphere® beads (32 μg) in the same TrisHCl buffer (320 μL final volume) and stirred for 2 h at 25 °C. The beads were immobilized (magnet) and the supernatant removed (*fluorescence analysis 1*). The solid residue was resuspended in 320 μL of TBS 1X buffer, heated for 10 min at 90 °C (gentle stirring 800 r.p.m.) and then centrifuged for 2 min at 8900 rpm. The supernatant was taken up for analysis (magnet immobilization), after being distributed in 3 wells (100 μL each) of a 96-well plate, using a ClarioStar® machine (BMG Labtech) equipped with FAM filters (λex = 492 nm; λem = 516 nm) (*fluorescence analysis 2*). Competitive experiments were carried out with labeled oligonucleotide (1 μM), 10 μM TASQ and in the presence of the unlabeled competitor ds12 (20 mol. equiv.). Data were analyzed with Excel (Microsoft Corp.) and OriginPro®9.1 (OriginLab Corp.); normalized FAM emission values are means of 3 measurements, according to the following methodology: *i- fluorescence analysis 1*: each analysis originated in 3 different experiments, performed as triplicates: a/ 3 control wells in which the F-ON was alone, whose FAM emission was normalized to 100; b/ 3 wells in

which F-ON was mixed with beads, in order to quantify the non-specific F-ON/bead binding; and c/ 3 wells in which F-ON and **BioTASQ/BioCyTASQ** were mixed with beads, in order to quantify the specific F-ON/**TASQ**/bead binding. *ii- fluorescence analysis 2*: each analysis originated in 2 different experiments, performed as triplicates: a/ 3 control wells comprising solutions that resulted from experiments performed with F-ON and beads, in order to quantify the non-specific F-ON/bead binding, the FAM emission of the solution was normalized to 1; and b/ 3 wells comprising solutions that resulted from experiments performed with F-ON, **BioTASQ/BioCyTASQ** and beads, in order to quantify the actual **BioTASQ/BioCyTASQ** capture capability when compared to the control experiments.

Cell culture and imaging.

MCF7 cells were routinely cultured in 75 cm^2 tissue culture flasks (Nunc) at 37 °C in a humidified, 5% CO_2 atmosphere in Dulbecco's Modified Eagle Medium (DMEM) supplemented with 10% fetal bovine serum (FBS, Gibco) and 1% Penicillin-Streptomycin (Pen-Strep: 5.0 $U.mL^{-1}$ Pen/5.0 $\mu g.mL^{-1}$ Strep, Gibco) mixture. Cells were subcultured twice a week using standard protocols. Round coverslips (12 mm) were sterilised with 70% ethanol before cell seeding. MCF7 cells were seeded at a density of 6.10^4 cells per coverslip on chambered coverslips (24 well-plate) and allowed to recover overnight. In the case of live-cell labelling, cells were incubated with either **BioTASQ** or **BioCyTASQ** (1 µM, 24h) at 37 °C, washed once with PBS 1X, fixed and permeabilized with ice cold MeOH for 10 min at room temperature. In the case of post-fixation labeling, seeded cells were fixed and washed with PBS 1X (3x), then incubated with 1 µM either **BioTASQ** or **BioCyTASQ** for 1 h at 25°C, washed with PBS 1X (3 x 5 min), then incubated for 1 h at 25°C in a light-tight box with Streptavidin-Cy3 (1 µg/mL) and washed with PBS 1X (3 x 5 min) and once with H_2O. Cells were mounted onto glass microscope slides with Fluoromount-G (Southern Biotech) containing DAPI (2.5 µg/mL). The cells were imaged with a Leica TCS SP8 confocal laser-scanning microscope with a 63X oil objective, collected through the following channels: DAPI (excitation: 340-380 nm; emission: < 425 nm), GFP (excitation: 450-490 nm; emission: 500-550 nm) and Cy3 (excitation: 518-562 nm; emission: > 580 nm). Images were processed with ImageJ (https://fiji.sc).[65]

ASSOCIATED CONTENT

Supporting Information

The Supporting Information is available free of charge at https://pubs.acs.org/.

Generalities concerning the chemical synthesis (Page S1), along with a description of the instruments and methods used (Page S2), the detailed synthesis and characterizations of CyTASQ (Pages S3-S6, Figures S1-S5), additional characterizations for BioCyTASQ (Pages S7-11, Figures S6-S11), the preparation of the oligonucleotides (Page S11), and additional CD experiments (Page S12, Figure S12).

Funding

This work was supported by the Centre National de la Recherche Scientifique (CNRS), the Agence Nationale de la Recherche (ANR-17-CE17-0010-01; ANR-18-CE07-0017-03), the European Union (PO FEDER-FSE Bourgogne 2014/2020 programs, FEDER n° BG0021532) and the INSERM Plan Cancer 2014-2019 (n° 19CP117-00).

Notes

The authors declare no competing financial interest.

Acknowledgments

The authors thank S. Amor and K. Duskova for their help in the pretargeted imaging protocols, C. Arnould (INRAe, Agrosup UMR1347) and DImaCell (*Dispositif Inter-régional d'Imagerie Cellulaire*) for the help with and access to the microscope, and N. Chéron (Pasteur, ENS Paris) for the preliminary molecular dynamics (MDs) simulations performed with TASQs.

References

1. Mutter, M., and Vuilleumier, S. (1989) A Chemical Approach to Protein Design—Template-Assembled Synthetic Proteins (TASP), *Angew. Chem. Int. Ed. 28*, 535-554.
2. Mutter, M., Dumy, P., Garrouste, P., Lehmann, C., Mathieu, M., Peggion, C., Peluso, S., Razaname, A., and Tuchscherer, G. (1996) Template Assembled Synthetic Proteins (TASP) as Functional Mimetics of Proteins, *Angew. Chem. Int. Ed. 35*, 1482-1485.
3. Nikan, M., and Sherman, J. C. (2008) Template-assembled synthetic G-quartets (TASQs), *Angew. Chem. Int. Ed. 47*, 4900-4902.
4. Cram, D. J., Jaeger, R., and Deshayes, K. (1993) Host-guest complexation. 65. Hemicarcerands that encapsulate hydrocarbons with molecular weights greater than two hundred, *J. Am. Chem. Soc. 115*, 10111-10116.
5. Nikan, M., and Sherman, J. C. (2009) Cation-Complexation Behavior of Template-Assembled Synthetic G-Quartets, *Journal of Organic Chemistry 74*, 5211-5218.

6. Nikan, M., Patrick, B. O., and Sherman, J. C. (2012) Crystal Structure of a Template-Assembled Synthetic G-Quadruplex, *ChemBioChem 13*, 1413-1415.
7. Stefan, L., Guedin, A., Amrane, S., Smith, N., Denat, F., Mergny, J.-L., and Monchaud, D. (2011) DOTASQ as a prototype of nature-inspired G-quadruplex ligand, *Chem. Commun. 47*, 4992-4994.
8. Lejault, P., Duskova, K., Bernhard, C., Valverde, I. E., Romieu, A., and Monchaud, D. (2019) The scope of application of macrocyclic polyamines beyond metal chelation, *Eur. J. Org. Chem. 2019*, 6146-6157.
9. Dumy, P., Eggleston, I. M., Esposito, G., Nicula, S., and Mutter, M. (1996) Solution structure of regioselectively addressable functionalized templates: an NMR and restrained molecular dynamics investigation, *Biopolymers 39*, 297-308.
10. Dumy, P., Eggleston, I. M., Cervigni, S., Sila, U., Sun, X., and Mutter, M. (1995) A convenient synthesis of cyclic peptides as regioselectively addressable functionalized templates (RAFT), *Tetrahedron Lett. 36*, 1255-1258.
11. Murat, P., Gennaro, B., Garcia, J., Spinelli, N., Dumy, P., and Defrancq, E. (2011) The Use of a Peptidic Scaffold for the Formation of Stable Guanine Tetrads: Control of a H-bonded Pattern in Water, *Chem. Eur. J. 17*, 5791-5795.
12. Nikan, M., Bare, G. A. L., and Sherman, J. C. (2011) Synthesis of a water-soluble triazole-linked cavitand-guanosine conjugate, *Tetrahedron Lett. 52*, 1791-1793.
13. Bare, G. A. L., Liu, B., and Sherman, J. C. (2013) Synthesis of a Single G-Quartet Platform in Water, *J. Am. Chem. Soc. 135*, 11985-11989.
14. Neidle, S. (2016) Quadruplex Nucleic Acids as Novel Therapeutic Targets, *J. Med. Chem. 59*, 5987-6011.
15. Neidle, S. (2017) Quadruplex nucleic acids as targets for anticancer therapeutics, *Nat. Rev. Chem. 1*, 0041.
16. Murat, P., Bonnet, R., Van der Heyden, A., Spinelli, N., Labbe, P., Monchaud, D., Teulade-Fichou, M.-P., Dumy, P., and Defrancq, E. (2010) Template-Assembled Synthetic G-Quadruplex (TASQ): A Useful System for Investigating the Interactions of Ligands with Constrained Quadruplex Topologies, *Chem. Eur. J. 16*, 6106-6114.
17. Stefan, L., and Monchaud, D. (2019) Applications of guanine quartets in nanotechnology and chemical biology, *Nat. Rev. Chem. 3*, 650-668.
18. Haider, S. M., Neidle, S., and Parkinson, G. N. (2011) A structural analysis of G-quadruplex/ligand interactions, *Biochimie 93*, 1239-1251.
19. Mergny, J. L., Phan, A. T., and Lacroix, L. (1998) Following G-quartet formation by UV-spectroscopy, *FEBS Lett. 435*, 74-78.
20. Stefan, L., Denat, F., and Monchaud, D. (2011) Deciphering the DNAzyme Activity of Multimeric Quadruplexes: Insights into Their Actual Role in the Telomerase Activity Evaluation Assay, *J. Am. Chem. Soc. 133*, 20405-20415.
21. Xu, H.-J., Stefan, L., Haudecoeur, R., Sophie, V., Richard, P., Denat, F., Barbe, J.-M., Gros, C. P., and Monchaud, D. (2012) Porphyrin-templated synthetic G-quartet (PorphySQ): a second prototype of G-quartet-based G-quadruplex ligand, *Org. Biomol. Chem. 10*, 5212-5218.
22. Haudecoeur, R., Stefan, L., Denat, F., and Monchaud, D. (2013) A Model of Smart G-Quadruplex Ligand, *J. Am. Chem. Soc. 135*, 550-553.
23. Haudecoeur, R., Stefan, L., and Monchaud, D. (2013) Multitasking Water-Soluble Synthetic G-Quartets: From Preferential RNA-Quadruplex Interaction to Biocatalytic Activity, *Chem. Eur. J. 19*, 12739-12747.
24. Laguerre, A., Desbois, N., Stefan, L., Richard, P., Gros, C. P., and Monchaud, D. (2014) Porphyrin-Based Design of Bioinspired Multitarget Quadruplex Ligands, *ChemMedChem 9*, 2035-2039.
25. Laguerre, A., Stefan, L., Larrouy, M., Genest, D., Novotna, J., Pirrotta, M., and Monchaud, D. (2014) A Twice-As-Smart Synthetic G-Quartet: PyroTASQ Is Both a Smart Quadruplex Ligand and a Smart Fluorescent Probe, *J. Am. Chem. Soc. 136*, 12406-12414.
26. Zhou , J., Roembke, B. T., Paragi , G., Laguerre , A., Sintim, H. O., Fonseca Guerra , C., and Monchaud, D. (2016) Computational understanding and experimental characterization of twice-as-smart quadruplex ligands as chemical sensors of bacterial nucleotide second messengers, *Sci. Rep. 6*, 33888.
27. Laguerre, A., Hukezalie, K., Winckler, P., Katranji, F., Chanteloup, G., Pirrotta, M., Perrier-Cornet, J.-M., Wong, J. M., and Monchaud, D. (2015) Visualization of RNA-quadruplexes in live cells, *J. Am. Chem. Soc. 137*, 8521-8525.
28. Laguerre, A., Wong, J. M. Y., and Monchaud, D. (2016) Direct visualization of both DNA and RNA quadruplexes in human cells via an uncommon spectroscopic mechanism, *Sci. Rep. 6*, 32141.
29. Yang, S. Y., Lejault, P., Chevrier, S., Boidot, R., Robertson, A. G., Wong, J. M., and Monchaud, D. (2018) Transcriptome-wide identification of transient RNA G-quadruplexes in human cells, *Nat. Commun. 9*, 4730.

30. Renard, I., Grandmougin, M., Roux, A., Yang, S. Y., Lejault, P., Pirrotta, M., Wong, J. M. Y., and Monchaud, D. (2019) Small-molecule affinity capture of DNA/RNA quadruplexes and their identification in vitro and in vivo through the G4RP protocol, *Nucleic Acids Res. 47*, 5502-5510.
31. Rousselin, Y., Sok, N., Boschetti, F., Guilard, R., and Denat, F. (2010) Efficient Synthesis of New C-Functionalized Macrocyclic Polyamines, *Eur. J. Org. Chem. 2010*, 1688-1693.
32. Renciuk, D., Zhou, J., Beaurepaire, L., Guedin, A., Bourdoncle, A., and Mergny, J.-L. (2012) A FRET-based screening assay for nucleic acid ligands, *Methods 57*, 122-128.
33. De Cian, A., Guittat, L., Kaiser, M., Sacca, B., Amrane, S., Bourdoncle, A., Alberti, P., Teulade-Fichou, M.-P., Lacroix, L., and Mergny, J.-L. (2007) Fluorescence-based melting assays for studying quadruplex ligands, *Methods 42*, 183-195.
34. Varshney, D., Spiegel, J., Zyner, K., Tannahill, D., and Balasubramanian, S. (2020) The regulation and functions of DNA and RNA G-quadruplexes, *Nat. Rev. Mol. Cell Biol. 21*, 459-474.
35. Mueller, S., Kumari, S., Rodriguez, R., and Balasubramanian, S. (2010) Small-molecule-mediated G-quadruplex isolation from human cells, *Nat. Chem. 2*, 1095-1098.
36. Sakahara, H., and Saga, T. (1999) Avidin–biotin system for delivery of diagnostic agents, *Adv. Drug Delivery Rev. 37*, 89-101.
37. Lesch, H. P., Kaikkonen, M. U., Pikkarainen, J. T., and Ylä-Herttuala, S. (2010) Avidin-biotin technology in targeted therapy, *Expert opinion on drug delivery 7*, 551-564.
38. Altai, M., Membreno, R., Cook, B., Tolmachev, V., and Zeglis, B. M. (2017) Pretargeted imaging and therapy, *Journal of Nuclear Medicine 58*, 1553-1559.
39. Moruno-Manchon, J. F., Lejault, P., Wang, Y., McCauley, B., Honarpisheh, P., Scheihing, D. A. M., Singh, S., Dang, W., Kim, N., Urayama, A., Zhu, L., Monchaud, D., McCullough, L. D., and Tsvetkov, A. S. (2020) Small-molecule G-quadruplex stabilizers reveal a novel pathway of autophagy regulation in neurons, *eLife 9*, e52283.
40. Lejault, P., Moruno-Manchon, J. F., Vemu, S. M., Honarpisheh, P., Zhu, L., Kim, N., Urayama, A., Monchaud, D., McCullough, L. D., and Tsvetkov, A. S. (2020) Regulation of autophagy by DNA G-quadruplexes, *Autophagy*, 1-8.
41. Chiarella, S., De Cola, A., Scaglione, G. L., Carletti, E., Graziano, V., Barcaroli, D., Lo Sterzo, C., Di Matteo, A., Di Ilio, C., and Falini, B. (2013) Nucleophosmin mutations alter its nucleolar localization by impairing G-quadruplex binding at ribosomal DNA, *Nucleic Acids Res. 41*, 3228-3239.
42. Mestre-Fos, S., Penev, P. I., Suttapitugsakul, S., Hu, M., Ito, C., Petrov, A. S., Wartell, R. M., Wu, R., and Williams, L. D. (2019) G-Quadruplexes in Human Ribosomal RNA, *J. Mol. Biol. 431*, 1940-1955.
43. Mestre-Fos, S., Ito, C., Moore, C. M., Reddi, A. R., and Williams, L. D. (2020) Human ribosomal G-quadruplexes regulate heme bioavailability, *J. Biol. Chem. 295*, 14855-14865.
44. Lyu, K., Chow, E. Y.-C., Mou, X., Chan, T.-F., and Kwok, Chun K. (2021) RNA G-quadruplexes (rG4s): genomics and biological functions, *Nucleic Acids Res.*
45. Umar, M. I., Ji, D., Chan, C.-Y., and Kwok, C. K. (2019) G-Quadruplex-Based Fluorescent Turn-On Ligands and Aptamers: From Development to Applications, *Molecules 24*, 2416.
46. Monchaud, D. (2020) Quadruplex detection in human cells, In *Annu. Rep. Med. Chem.* (Neidle, S., Ed.), pp 133-160, Academic Press.
47. Kwok, C. K., and Merrick, C. J. (2017) G-quadruplexes: prediction, characterization, and biological application, *Trends Biotechnol. 35*, 997-1013.
48. Spiegel, J., Adhikari, S., and Balasubramanian, S. (2020) The structure and function of DNA G-quadruplexes, *Trends Chem. 2*, 123-136.
49. Raguseo, F., Chowdhury, S., Minard, A., and Di Antonio, M. (2020) Chemical-biology approaches to probe DNA and RNA G-quadruplex structures in the genome, *Chem. Commun. 56*, 1317-1324.
50. Cañeque, T., Müller, S., and Rodriguez, R. (2018) Visualizing biologically active small molecules in cells using click chemistry, *Nat. Rev. Chem. 2*, 202-215.
51. Chambers, V. S., Marsico, G., Boutell, J. M., Di Antonio, M., Smith, G. P., and Balasubramanian, S. (2015) High-throughput sequencing of DNA G-quadruplex structures in the human genome, *Nat. Biotechnol. 33*, 877-881.
52. Kwok, C. K., Marsico, G., Sahakyan, A. B., Chambers, V. S., and Balasubramanian, S. (2016) rG4-seq reveals widespread formation of G-quadruplex structures in the human transcriptome, *Nat. Meth. 13*, 841-844.
53. Kwok, C. K., Marsico, G., and Balasubramanian, S. (2018) Detecting RNA G-Quadruplexes (rG4s) in the Transcriptome, *Cold Spring Harbor Persp. Biol. 10*, a032284.
54. Todd, A. K., Johnston, M., and Neidle, S. (2005) Highly prevalent putative quadruplex sequence motifs in human DNA, *Nucleic Acids Res. 33*, 2901-2907.

55. Huppert, J. L., and Balasubramanian, S. (2005) Prevalence of quadruplexes in the human genome, *Nucleic Acids Res. 33*, 2908-2916.
56. Bedrat, A., Lacroix, L., and Mergny, J.-L. (2016) Re-evaluation of G-quadruplex propensity with G4Hunter, *Nucleic Acids Res. 44*, 1746-1759.
57. Hänsel-Hertsch, R., Beraldi, D., Lensing, S. V., Marsico, G., Zyner, K., Parry, A., Di Antonio, M., Pike, J., Kimura, H., and Narita, M. (2016) G-quadruplex structures mark human regulatory chromatin, *Nat. Genet. 48*, 1267-1272.
58. Hänsel-Hertsch, R., Spiegel, J., Marsico, G., Tannahill, D., and Balasubramanian, S. (2018) Genome-wide mapping of endogenous G-quadruplex DNA structures by chromatin immunoprecipitation and high-throughput sequencing, *Nat. Protoc. 13*, 551-564.
59. Hänsel-Hertsch, R., Simeone, A., Shea, A., Hui, W. W., Zyner, K. G., Marsico, G., Rueda, O. M., Bruna, A., Martin, A., and Zhang, X. (2020) Landscape of G-quadruplex DNA structural regions in breast cancer, *Nat. Genet.*, 1-6.
60. Zheng, K.-w., Zhang, J.-y., He, Y.-d., Gong, J.-y., Wen, C.-j., Chen, J.-n., Hao, Y.-h., Zhao, Y., and Tan, Z. (2020) Detection of genomic G-quadruplexes in living cells using a small artificial protein, *Nucleic Acids Res. 48*, 11706-11720.
61. Rhodes, D., and Lipps, H. J. (2015) G-quadruplexes and their regulatory roles in biology, *Nucleic Acids Res. 43*, 8627-8637.
62. Kim, N. (2019) The interplay between G-quadruplex and transcription, *Curr. Med. Chem. 26*, 2898-2917.
63. del Mundo, I. M., Vasquez, K. M., and Wang, G. (2019) Modulation of DNA structure formation using small molecules, *Biochim. Biophys. Acta - Mol. Cell Res.*, 118539.
64. Maizels, N. (2015) G4-associated human diseases, *EMBO Rep.*, e201540607.
65. Schindelin, J., Arganda-Carreras, I., Frise, E., Kaynig, V., Longair, M., Pietzsch, T., Preibisch, S., Rueden, C., Saalfeld, S., Schmid, B., Tinevez, J.-Y., White, D. J., Hartenstein, V., Eliceiri, K., Tomancak, P., and Cardona, A. (2012) Fiji: an open-source platform for biological-image analysis, *Nat. Meth. 9*, 676-682.